sustainability

MDPI

Article

Efficiency Enhancement of a Hybrid Sustainable Energy Harvesting System Using HHHOPSO-MPPT for IoT Devices

Sirine Rabah [1], Aida Zaier [2], Jaime Lloret [3,*] and Hassen Dahman [4,5]

[1] MACS Laboratory LR 16ES22, National Engineering School of Gabes, University of Gabes, Omar ibn Elkhattab Street, Zrig Eddakhlania 6029, Tunisia
[2] LR-11/TIC-03 Innov'COM Laboratory, Higher School of Communication of Tunis, University of Carthage, Ariana 2083, Tunisia
[3] Instituto de Investigacion para la Gestion Integrada de Zonas Costeras, Universitat Politecnica de Valencia, 46730 Gandia, Spain
[4] LaPhyMNE Laboratory (LR05ES14), FS Gabes, University of Gabes, Gabes 6029, Tunisia; h_dahman_2000@yahoo.com
[5] Department of Electrical Engineering, National Engineering School of Gabes, University of Gabes, Gabes 6029, Tunisia
* Correspondence: jlloret@dcom.upv.es

Abstract: The Internet of Things (IoT) is a network of interconnected physical devices, vehicles, and buildings that are embedded with sensors, software, and network connectivity, enabling them to collect and exchange data. This exchange of data between the physical and digital worlds allows for a wide range of applications, from smart homes and cities to industrial automation and healthcare. However, a key challenge faced by IoT nodes is the limited availability of energy to support their operations. Typically, these nodes can only function for a few days based on their duty cycle. This paper introduces a solution that aims to ensure the sustainability of IoT applications by addressing this energy challenge. Thus, we develop a design of a hybrid sustainable energy system designed specifically for IoT nodes, using solar photovoltaic (PV) and wind turbines (WT) chosen for their multiple benefits and complementarity. The system uses the single-ended primary-inductance converter (SEPIC) and is controlled using a hybrid approach, combining Harris Hawks Optimization and Particle Swarm Optimization (HHHOPSO). Each SEPIC converter boost the electrical energy generated to attain the required voltage level when charging the battery. The proposed methodology is implemented in MATLAB/Simulink and its performance is measured using appropriate metrics. In terms of efficiency and average power, the results show that the suggested method outperforms previous strategies. Our system powers also many sensor nodes, leading to a high level of sustainability and lowering the carbon footprint associated with traditional energy sources.

Keywords: IoT; energy harvesting; PV; WT; SEPIC; PSO; HHO

Citation: Rabah, S.; Zaier, A.; Lloret, J.; Dahman, H. Efficiency Enhancement of a Hybrid Sustainable Energy Harvesting System Using HHHOPSO-MPPT for IoT Devices. *Sustainability* **2023**, *15*, 10252. https://doi.org/10.3390/su151310252

Academic Editor: Nallapaneni Manoj Kumar

Received: 20 May 2023
Revised: 19 June 2023
Accepted: 25 June 2023
Published: 28 June 2023

1. Introduction

The increase of Internet of Things devices has a significant impact on society, particularly in the fields of healthcare, entertainment, personal communication, and environmental monitoring [1–3]. One of the significant challenges faced by these low-power devices is their reliance on batteries that require frequent charging or replacement. This challenge has led to the emerging technology of energy harvesting as an attractive alternative solution for IoT devices. Energy harvesting refers to the process of transforming various types of energy resources, such as temperature, vibration, pressure and electromagnetic radiation including light and RF waves into usable electrical energy. In recent years, there has been a growing need for sustainable energy sources due to the increasing demand for clean energy production with minimal environmental impact. One of the most promising alternatives to traditional fossil fuels is hybrid energy harvesting, which combines multiple renewable

sources such as solar and wind power. It is anticipated that integrating both PV and wind energy harvesting can yield significant benefits in terms of enhancing the lifetime of IoT sensors, owing to their complementary nature [4]. In cases where one energy source is insufficient or unavailable, the other energy source can compensate to meet storage battery demands. However, the output of these two energy sources can be uncertain due to factors such as environmental conditions or day-night variations. To achieve a stable voltage output, these two systems are connected in parallel to one another, so that if one source is unavailable, the system can be balanced by the other. As such, both systems can function independently or simultaneously. Due to the variable nature of solar radiation and wind speed, the present PV/wind arrangement has limited conversion capability [5]. Factors such as radiation level, temperature, and wind speed all have a significant impact on the performance of PV panels and wind turbines. As a result, additional Maximum Power Point Tracking (MPPT) approaches are urgently needed to achieve higher efficiency, maximize power extraction from PV panels and wind turbines and ensure optimal performance. A range of techniques has been developed for this purpose [6]. The constant voltage method is used in hybrid solar-wind energy systems to achieve a consistent voltage during battery charging [7]. Nonetheless, this method produces significant oscillations and necessitates a lengthy convergence time. On the other hand, the Perturb and Observe (P&O) algorithm serves as an active power control in a hybrid system and demonstrates strong dynamic performance in response to variations in wind and solar irradiation [8]. P&O modifications involving step size changes have also been performed and implemented in the hybrid system [9]. The incremental conductance method is also utilized in hybrid systems [10]. Traditional MPPT approaches have drawbacks such as dynamic response concerns and steady-state oscillation issues, which make them ineffective in adjusting to changing environmental conditions [11]. To address these issues, academics have created clever and advanced processing systems that employ techniques such as genetic algorithms (GA), neural networks (NN), and fuzzy logic controllers (FLC). However, the use of FLC, GA, and NN techniques for intelligent MPPT controllers in hybrid solar-wind systems is frequently limited due to variables such as limited fuzzy deduction rules [12] small population numbers, and limited data availability. While these techniques function well under specific conditions, they may fail to monitor the Maximum Power Point (MPP) precisely when facing fluctuations in the power curve [13,14]. In PV-wind system, efficient extraction of the maximum power point is critical. As a result, the purpose of this work is to devise an efficient way for accomplishing this goal.

The main contributions of this work can be listed as follows:

- The power is generated from a hybrid sustainable energy system that combines solar and wind power to supply the IoT node for the communication process, and the power is charged in the Lithium battery of 3.7 V.
- The generated power is then fed into a SEPIC converter, which is responsible of converting the voltage amplitude to the desired level. To maximize the energy production from both solar and wind turbine sources, the MPPT algorithm is applied.
- An energy-efficient algorithm that combines Particle Swarm Optimization (PSO) and Harris Hawks Optimization (HHO) methodologies is used to optimize the MPPT to track appropriately the maximum power from both the solar and wind sources. The maximum power generated from these sources is given then to the IoT nodes.

This document is structured as follows: Section 2 provides an overview on the MPPT technique in solar-wind systems. Section 3 includes a thorough discussion of solar and wind energy harvesting technologies. Section 4 provides detailed information on the design of our proposed hybrid solar-wind energy harvesting system, including the modeling of solar and wind components, the SEPIC converter and the rechargeable battery. Section 5 discusses the MPPT principle and outlines the chosen control algorithm. Section 6 presents information on IoT devices and network lifetime. Section 7 provides the results of our research and provides a corresponding discussion. Finally, Section 8 highlights the main findings of our research.

2. Literature Review

This section includes an overall review of the existing literature on the Maximum Power Point Tracking (MPPT) technique in solar-wind systems.

S. Mahdi et al. [15] demonstrated the performance of the MSX-64 PV module with a boost DC-DC converter for MPPT applications. The paper investigates three MPPT techniques under partial shadowing and real-world weather conditions. The results focus on energy efficiency, rising time, the ability to track global MPP, and reactivity to changing weather. The results show that the MPPT techniques are excellent at simulating MPP during partial shading and adapting to changing weather conditions.

V. Dhanunjaya et al. [16] introduced the Cuckoo search MPPT Algorithm (CSA) for Maximum Power Point Tracking (MPPT) in a PV-Wind hybrid system. Traditional MPPT algorithms struggle with changing environmental variables, making CSA an appropriate evolutionary algorithmic technique. The suggested system integrates DC-DC step-up boost converters and successfully optimizes power under different irradiance situations using simulation findings.

Preeti Gupta et al. [17] introduced an improved solar energy harvesting system for wireless sensor networks (WSNs) based on Maximum Power Point Tracking (MPPT) and the Emperor Penguin Optimization (EPO) algorithm. The system employs solar photovoltaic energy and a SEPIC converter to extend network lifetime by harvesting and storing solar energy efficiently. The system powers several sensor nodes, allowing for longer operation and improving overall WSN performance.

Hai, Tao, et al. [18] proposed an intelligent power extraction approach for a grid-connected hybrid generating system. It combines a fuzzy gain scheduling PD controller and radial basis function network sliding mode control. The setup consists of a wind turbine and a solar panel. The suggested technique exhibits efficient and accurate tracking of maximum generated power, with the added benefits of pitch angle control for the wind turbine and protection against catastrophic operations. The suggested controller's effectiveness is validated by simulation results using MATLAB.

Linus A. Aloo et al. [19] presented the modeling of a PV-Wind hybrid microgrid with a Battery Energy Storage System (BESS) is discussed in this literature review, and a Genetic Algorithm-Adaptive Neuro-Fuzzy Inference System (GAANFIS) controller for voltage management is proposed. When compared to other controllers, the GA-ANFIS outperforms them in terms of rise time, settling time, overshoot, and nonlinear handling capacity.

A. Renjith et al. [20] presented a hybrid system for sustainable power generation that combines Photovoltaic (PV) and Wind Turbine (WT) technology. The system addresses the issue of partial shading in power generation and presents a hybrid technique for maximum power extraction and compensation utilizing the Adaptive Neuro Fuzzy Interference System-Honey Badger Algorithm (ANFIS-HBA). MATLAB simulations show that the suggested method outperforms other approaches in terms of power tracking under various partial shading conditions.

Ahmed Hussain Elmetwaly et al. [21] proposed a new MPPT strategy based on jellyfish search optimization (JSO). In addition, the study offers a unified power-quality conditioner (UPQC) to improve microgrid performance and handle power-quality concerns. The proposed algorithm's effectiveness is compared to previous MPPT algorithms, and four case studies are completed to validate the benefits brought by the new UPQC. The research findings illustrate the proposed approach's high performance, which is demonstrated through simulation with the MATLAB/Simulink program and experimental tests with PV module simulation models.

In our proposal, we aim to fill the gap between existing studies on hybrid solar and wind systems and their application in IoT sensors. While previous research has explored the potential of combining solar and wind energy sources, there is a lack of focus on integrating these systems specifically for IoT applications. Our proposal fills this gap by designing a sustainable energy system tailored for IoT sensors, using the advantages of both solar photovoltaic (PV) and wind turbines (WT). Additionally, our optimization algorithm, which

integrates Particle Swarm Optimization (PSO) and Harris Hawks Optimization (HHO), offers improved efficiency in maximizing power generation and mitigating energy wastage. By incorporating these elements, our proposal presents a comprehensive and innovative solution that enhances the overall performance of IoT networks powered by renewable energy sources.

Moreover, the integration of solar PV and wind turbines within the specific domain of this study offers several significant contributions. These include adaptation to IoT requirements, enabling sustainable and renewable energy sources that are specifically adjusted to efficiently power IoT devices. The incorporation of solar PV and wind turbines also provides network independence, allowing IoT networks to operate autonomously without relying on traditional power sources, thus extending their operational lifespan. This integration promotes environmental sustainability by reducing reliance on fossil fuels and minimizing the environmental impact. Additionally, the energy efficiency of solar PV and wind turbines enables optimal power utilization for IoT devices, leading to reduced energy consumption and increased overall system efficiency.

Furthermore, these technologies offer scalability and flexibility, making them adaptable to different IoT applications and environments. They can be deployed in various settings, ranging from urban to remote locations, supporting the growth and expansion of IoT networks. In terms of cost-effectiveness, solar PV and wind turbines have the potential to reduce operational costs associated with traditional energy sources, providing long-term cost savings and enhancing the economic feasibility of deploying IoT networks.

To sum up, these contributions improve the overall performance, reliability and sustainability of IoT networks that use renewable energy sources.

3. Energy Harvesting Techniques

The drawbacks of using batteries, such as environmental pollution, have prompted the exploration of alternative methods to power IoT sensors with the energy available in their surroundings, a process known as energy harvesting. The main advantage of this technology is the continuity of the power supply. Theoretically, it lasts to operate as long as there is energy in the environment [22–24]. The future society, which largely relies on energy, highly depends on energy harvesting technology. This is mostly due to the fact that energy may be obtained from a variety of sources, as seen in Figure 1, making it a ubiquitous and environmentally friendly process. Moreover, the maintenance costs associated with such systems are relatively low. There are numerous sources of ambient energy that can be used with energy harvesting technology, some of which occur naturally and others human-generated [25]. These energy sources are gaining increasing attraction in the literature, including vibrations energy, radio frequency energy, thermal energy, solar photovoltaic energy (indoor and outdoor), and wind energy.

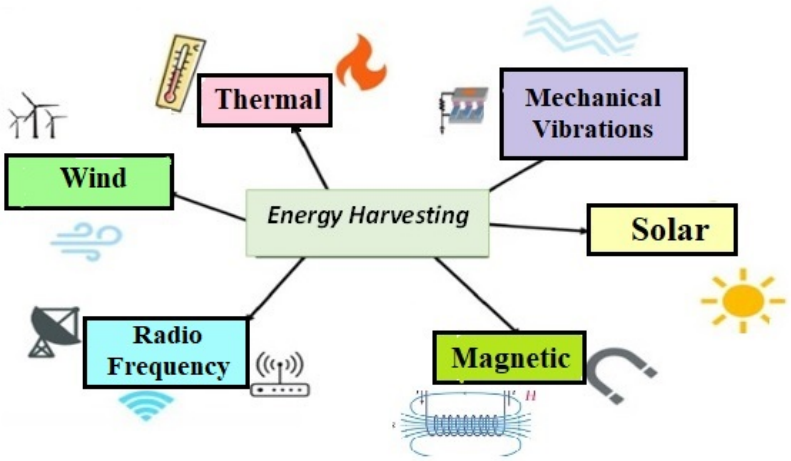

Figure 1. Energy harvesting sources.

3.1. Solar Energy Harvesting

Light is a plentiful energy source that can power a variety of indoor and outdoor applications, including wireless sensors and devices in the burgeoning IoT industry. To capture sunlight, solar or photovoltaic (PV) cells made of semiconductor materials such as silicon can be used. Through the photovoltaic effect, this technology directly converts sunlight into usable electricity. The semiconductor absorbs the energy of the photons, causing electrons to move out of their regular positions and create holes. This generates a current flow for the electric circuit. A photovoltaic cell forces the electrons and holes to move forward in opposite directions, creating a voltage and current between the two parts, like a battery. Sunlight is the most suitable energy source for harvesting, estimated to provide 1.4 kW/m^2 [26]. While the theoretical efficiency of a PV cell is 90%, the practical efficiency is around 40% [27]. PV cells can maintain high performance for up to 25 years, after which the generated power decreases. Recently, numerous solar energy harvesting (SEH) prototypes have been developed for WSN and IoT networks. In building management, a WSN system designed with a Tyndall 25 mm mote uses energy harvesting from indoor light via a photovoltaic cell to reduce energy consumption [28]. An intelligent SEH system for WSN nodes is proposed in [29], utilizing a hardware-based comparator circuit to manage battery charging for increased system robustness. The potential of solar cells to supply energy for a single node is examined in detail in [30], including discussions on cell characteristics and control circuit design for battery voltage regulation. Sharma et al. conduct a comprehensive survey on SEH for WSN nodes in [31], covering solar cell efficiency, DC-DC converters, MPPT, energy prediction algorithms, and design challenges and solutions. An efficient SEH system with MPPT and PWM techniques is proposed in [31], with simulation, optimization, and hardware implementation. A wireless sensor system utilizing solar energy harvesting for agriculture development is proposed in [32]. The HaLOEWEn solar energy harvester charges a 4.6 AH Li-ion battery using tiny solar panels, and the quantity of energy harvested is determined by the prevailing light conditions [33]. A flexible wearable body sensor node with indoor photovoltaic energy harvesting is designed in [34], while solar micro panels placed in shirts tissue are used to harvest energy in [35].

3.2. Wind Energy Harvesting

Wind energy, similarly to solar energy, can be harnessed to produce usable electricity. While solar energy is dependent on sunlight, wind energy can be accessible during the day and night, as well as in rainy and cloudy conditions. Windy regions, including civil structures such as bridges and high buildings, are potential sources for wind energy harvesting for wireless sensor nodes. Researchers have explored the feasibility of wind energy harvesting, and numerous studies in this field have been carried out. For instance, Park et al. designed a bridge health monitoring system in [36] that used a wireless sensor node powered by a wind turbine generator (WTG). With a maximum output power of 27.3 mW at 3.0 m/s wind speed, the WTG generated enough electricity to power the wireless sensor node. Another work in [37] addressed the development of a small wind energy harvester with MPPT for monitoring wildfires with wireless sensor nodes. In [38], an anemometer-based solution was used to harvest wind energy, where the motion of an anemometer shaft was used to generate energy. The harvested energy was converted to battery potential using a pulsed buck-boost converter, and trickle charging was used to power the battery. The analysis showed that the energy harvesting capability ranged from ten to hundreds of micro-watts up to approximately one milli watt, which could significantly extend the lifetime of sensor devices.

4. Proposed Energy Harvesting Design for IoT Devices

When solar and wind energy sources are combined, a hybrid power system is created to provides numerous advantages over a single system. The ability to integrate the outputs of both solar and wind energy systems in parallel, compensating for the absence of either system, is a significant advantage of this system. Furthermore, within the hybrid power

system, both of the energy sources can operate independently or in tandem. The solar system consists of a photovoltaic panel, while the wind turbine system includes a PMSG and a rectifier. The SEPIC converter is used to boost the input generated power from both the PV and wind turbine. Hence, an effective MPPT algorithm based on the Hybrid of HHO and PSO (HHHOPSO) is developed to extract the maximum power from the hybrid solar-wind system. The proposed hybrid approach is intended to achieve good tracking performance and quick convergence speed while minimizing computing costs and keeping the design structure simple. The output power from both converters can then be combined in a DC bus. A voltage control strategy is used to keep the DC bus voltage stable. This control strategy maintains the DC bus voltage within a specified range by adjusting the duty cycle of the SEPIC converters. This proposed energy harvesting system charges a rechargeable battery to ensure that the IoT devices are powered on. An IoT sensor node typically consists of a sensing unit, a microcontroller processing unit, and a communication unit. Figure 2 illustrates a block diagram of the hybrid solar-wind energy harvesting system that uses HHHOPSO MPPT to charge IoT nodes.

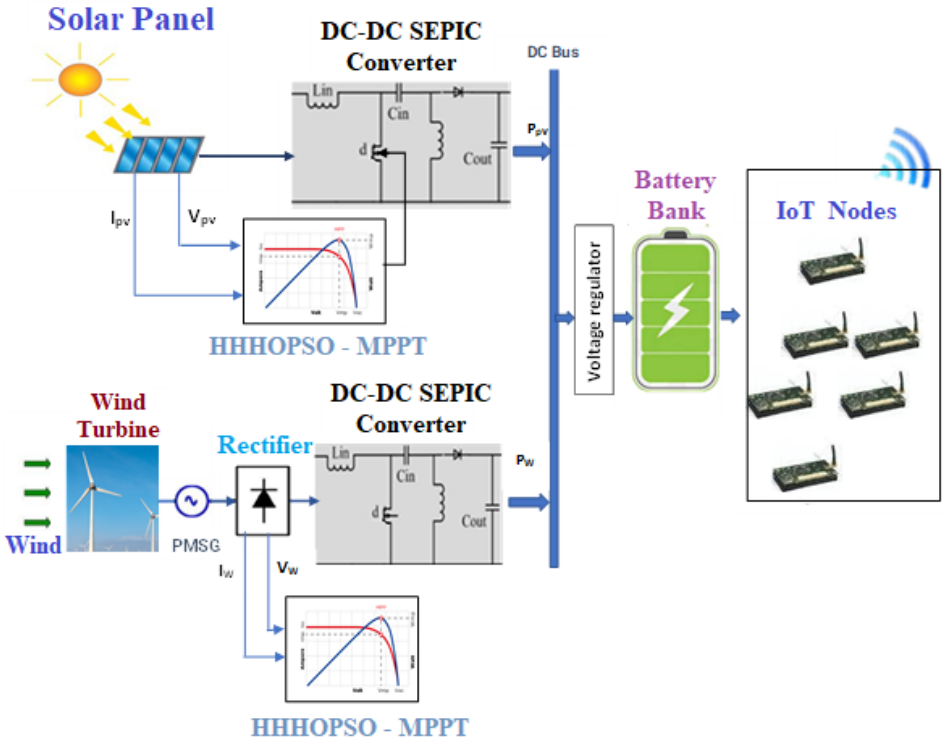

Figure 2. Block diagram of the proposed solar-wind hybrid system.

Thus, this research focuses on improving the power generation from solar and wind by using an energy-efficient technique in MPPT for enhancing the IoT network lifetime.

The following subsections provide detailed information on the various components of the proposed energy harvesting receiver design.

4.1. Modeling of Solar Photovoltaic Systems

This section will introduce the mathematical models of the solar PV component within the hybrid energy system proposed. To achieve the desired power output, PV modules are connected in series and parallel within the PV field. Each module comprises individual cells [39]. To model the PV field, we begin with the basic element, which is the cell. It can be seen as an ideal current source that provides a current, I_{ph}, proportional to the incident

light power, in parallel with a diode that is indicated by the P-N junction. Depending on Kirchhoff's current law, the equation for the output current is as follows [40]:

$$I = I_{ph} - I_D \tag{1}$$

The photo-current (I_{ph}) is directly proportional to the solar irradiation and temperature, as shown by this equation:

$$I_{ph} = [I_{sc} - K_i(T - T_{STC})]\frac{G}{G_{STC}} \tag{2}$$

where I_{sc} is the short-circuit current, K_i represents the short-circuit current temperature coefficient, G_{STC} and T_{STC} denote the irradiation and temperature values under standard test conditions, while G and T represent the actual values of irradiation and temperature. The module diode current can be determined using Equation (3), which is dependent on the saturation current I_0:

$$I_D = I_0(\exp\frac{V_D}{V_{th}} - 1) \tag{3}$$

Here, V_D represents the voltage diode, and $V_{th} = \frac{(A \times K \times T)}{q}$ represents the thermal voltage. The saturation current is given by:

$$I_0 = I_{rs}(\frac{T}{T_{STC}})^3 \exp[\frac{q \times E_g}{A \times k}(\frac{1}{T_{STC}} - \frac{1}{T})] \tag{4}$$

With $q = (1.6 \times 10^{-19}C)$ being the electron charge, $K = 1.38 \times 10^{-23}$ J/k being the Boltzmann's constant, $(A = 2)$ being the diode ideality factor, $E_g \simeq 1.1$ eV at $T = 25\ ^\circ$C being the semiconductor band-gap energy, and I_{rs} being the reverse saturation current.

When selecting a solar panel, it is crucial to consider various parameters, such as open circuit voltage (V_{oc}), short circuit current (I_{sc}), maximum output power (P_{max}), and the surface area. Additionally, durability is important to withstand outdoor conditions and minimize replacement costs. Taking all these factors into account, we have chosen solar panel for simulating a low power device according to the specifications provided in Table 1.

Table 1. Technical characteristics of the solar panel used.

Parameter	Value
Open circuit voltage (V_{oc})	5.6 V
Short circuit current (I_{sc})	660 mA
Maximum output power (P_{max})	2.4 W
Voltage at maximum power (V_{mp})	4 V
Current at maximum power (I_{mp})	600 mA
Surface area	36 cm^2

4.2. Modeling of Wind System

The wind turbine system is designed to transform the wind's kinetic energy into mechanical energy, which is then transferred into electrical energy by a generator. A rectifier then converts the electrical energy into direct current (DC) [41]. The generated power in a steady condition is expressed as follows:

$$P_{mc} = \frac{1}{2}C_p(\lambda, \beta)\rho_{AD}\pi R_{bd}^2 V_W^3 \tag{5}$$

The air density (ρ_{AD} = 1.225 kg/m^3), the turbine radius (R_{bd} in meters), the wind speed (V_W in m/s), the turbine performance coefficient (C_p), the ratio of the rotor blade speed to the wind velocity (λ), and the blade pitch angle (β) are all included in the wind power Equation (5). Increasing the value of C_p is essential to maximize the output power of a wind

turbine. The coefficient of performance is strongly influenced by the "Tip Speed Ratio", which exhibits a nonlinear relationship and depends on factors such as blade quantity, pitch, and shape. The maximum attainable value for C_p is approximately 59%, often referred to as the Betz limit. The speed ratio λ is defined as follows:

$$\lambda = \frac{\Omega R_{bds}}{V_W} \tag{6}$$

The following formula is used to determine the turbine's output torque:

$$T_{mc} = \frac{P_{mc}}{\Omega} = \frac{1}{2}\frac{C_p(\lambda,\beta)\rho_{AD}\pi R_{bd}^2 V_W^3}{\Omega} \tag{7}$$

The power coefficient is at its highest value $C_{pM} = C_p(\lambda_{opt})$ if the speed ratio is kept at its ideal value λ_{opt}. In this case, the wind turbine's maximum power production can be calculated as follows:

$$P_m^{opt} = \frac{1}{2}C_{pM}\rho\pi R_{bd}^2 V_W^3 \tag{8}$$

The ideal rotor speed can be determined as follows when the speed ratio is expected to be maintained at the ideal value:

$$\lambda^{opt} = \frac{\Omega R_{bd}}{V_W} \Rightarrow \Omega^{opt} = \frac{\lambda^{opt} V_W}{R_{bd}} \tag{9}$$

Thus, there is an optimal rotor speed Ω^{opt} that optimizes the power output for each wind speed.

In our system, we used a commercial wind turbine toy to generate wind power. The manufacturer claims it to be the "World's smallest wind turbine" [42]. Although the manufacturer did not provide any performance data, the same turbine was tested in a separate study [37]. This last provides valuable information regarding the performance of the wind turbine, offering then insights of its abilities and efficiency.

4.3. Modeling of SEPIC Converter

A SEPIC converter's output voltage may differ from the input voltage because it can be either higher or lower [43]. Figure 3 depicts the SEPIC converter, which uses two inductors, L1 and L2, wound on the same core and subjected to the same voltages throughout the switching cycle. The output voltage of the SEPIC converter controls the MOSFET duty cycle. When the switch is depressed, the output voltage falls to 0 V. The SEPIC converter is notably useful in battery charging applications, where the voltage can be below or above the regulator's output.

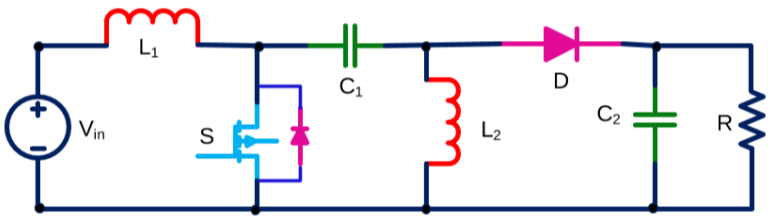

Figure 3. SEPIC converter circuit.

The output voltage of a SEPIC converter is typically expressed as:

$$V_{out} = \frac{D}{D-1}V_{in} \tag{10}$$

where V_{out} is the output voltage, V_{in} is the input voltage, and D is the duty cycle.

The SEPIC converter duty cycle (D) in continuous conduction mode (CCM) is given by the following equation:

$$D = \frac{V_{out} + V_D}{V_{in} + V_{out} + V_D} \tag{11}$$

The voltage across the diode can be denoted as V_D, and the maximum duty cycle can be expressed as:

$$D_{max} = \frac{V_{out} + V_D}{V_{IN(Min)} + V_{out} + V_D} \tag{12}$$

The symbol $V_{IN(Min)}$ represents the minimum input voltage.

In this paper we used two SEPIC converters. The first one is connected to the solar system with an input voltage of 4 V. The second one is connected to the wind system with an input voltage of 3.5 V.

Rechargeable Battery

There are primarily two types of energy storage devices in IoT networks: batteries and supercapacitors. Rechargeable batteries are widely used in both solar and wind energy systems and have higher energy densities than supercapacitors. For IoT networks, many rechargeable batteries have been commonly used, such as nickel-cadmium (NiCd), nickel-zinc (NiZn), nickel metal hydride (NiMH), and lithium-ion (Li-ion). In our proposed work, a lithium-ion battery of 740 mAh capacity and a nominal voltage of 3.7 V is used. This modern battery has several advantages over traditional rechargeable batteries, including a higher energy density, faster discharge rate, higher cell voltage, extended life cycle, and the absence of memory effects [44].

5. MPPT Technique

MPPT is a commonly used technique in solar and wind power systems to increase their efficiency. It entails tracking the maximum power peak of nonlinear electrical generators, such as solar photovoltaic and wind turbine generators. The power peak in wind systems is determined by the turbine size and wind speed passing through the rotor blades, whereas the power peak in solar systems is influenced by the sun radiation level and temperature range. Failure to track the power peak can result in damage to the interconnected system and power loss. The incremental conduction method, perturb and observe method, and current sweep method are some of the MPPT methods available, with different techniques tailored to specific system specifications. Although these methods offer maximum power from the solar and wind systems, they have drawbacks such as increased complexity, limited convergence, and more limitations. As a result, we employed the hybrid HHHOPSO approach, which has higher efficiency, better convergence and faster tracking. The effective model is particularly useful in actively tracking the MPP in both stable and unstable conditions.

5.1. Particle Swarm Optimization (PSO)

The concept of Particle Swarm Optimization (PSO) is inspired by natural phenomena, such as swarms of bees, schools of fish, or flocks of birds [45]. Swarm intelligence-based optimization techniques are considered evolutionary methods that are suitable for optimizing multivariate renewable systems. In this approach, a swarm of particles is initially distributed randomly in a multidimensional space, and they move collectively without any collision to search for optimal solutions, similar to the way swarms of animals search for shelter or food. Each particle utilizes its own intelligence and the collective intelligence of the swarm to remember the best position (P_{Best}) it has discovered. If one member of the swarm finds an optimal solution, others can quickly follow by modifying their position and velocity, which are given in Equations (13) and (14). Each particle's status is defined by

its position and velocity, with Equations (13) and (14) indicating the updating velocity and position, respectively [46,47].

$$V_i^{k+1} = \omega V_i^k + c_1 r_1 (X_{Pbesti}^K - X_i^k) + c_2 r_2 (X_{Gbesti}^k - X_i^k) \tag{13}$$

$$X_i^{k+1} = X_i^k + V_i^{k+1} \tag{14}$$

where ω is a constant called the inertia weight, c_1, c_2 represent acceleration constants, and r_1, r_2 represent random functions generated in the range [0, 1] at each iteration k. The steps of the PSO algorithm are outlined in Algorithm 1.

Algorithm 1 PSO

Inputs: Generate an initial random population with size N and PSO parameters (v, c_1, c_2 and w)
Outputs: The best solution X_{best}
Repeat
Compute the fitness value for each particle.
Determine the global best solution (X_{gbest}) and the personal best solution (X_{pbest})
Update the position of each solution using Equation (13).
Update the velocity of each solution using Equation (14).
(stop conditions)

5.2. Harris Hawks Optimization (HHO)

The HHO algorithm is based on the hunting process of Harris' hawks, in which they cooperate to capture their prey [48]. HHO is a population-based optimization algorithm that works without using gradients. The central concept of HHO is based on Harris hawks' cooperative hunting behavior, specifically their "surprise pounce" technique or "seven kill" strategy. During this approach, multiple hawks work together to attack the prey from various angles, creating confusion and making the prey easier to catch. The hawks' pursuit model influences the behavior of the prey during the chase, and the birds collaborate during the attack. The group's leader leads the initial attack, following the prey and then soaring out of sight, allowing the next Harris hawk to take command. These hawks' chasing patterns vary depending on the dynamics of the situation and the prey's escape strategy. This behavior is mathematically reproduced in order to create an optimization algorithm. The HHO algorithm is divided into two phases, the first of which is concerned with exploration ability and is written as follows.

5.2.1. Exploration Phase

During the exploration phase of the Harris Hawks Optimization (HHO) algorithm, the behavior of Harris hawks when attempting to track prey is replicated. They sit and wait for new prey, similar to how hawks represent candidate solutions, and the best solution identified thus far is the prey. To identify prey, these hawks sit in random locations and use two operations depending on a probability, q, obtained from Equation (15). Hawks orient themselves based on population and prey location if q is less than 0.5. If q is larger than or equal to 0.5, hawks perch at random on a tree.

$$X(k+1) = \begin{cases} X_{random}(k) - |X_{random}(k) - X_{r2}X(k)| & q \geq 0.5 \\ (X_{ra}(k) - X_p(k)) - r_3(LB + r_4(UB - LB)) & q < 0.5 \end{cases} \tag{15}$$

where the hawk's current position, $X(k)$, and the next position, $X(k+1)$, are calculated using the prey's position, $X_{ra}(k)$, and other random variables, such as q, r_1, r_2, r_3, and r_4. To determine the next position, the model chooses a position at random, $X_{random}(k)$, from the

available options and computes the average position of the existing positions, $X_p(t)$, using the equation:

$$X_p(k) = \frac{1}{N}\sum_{i=1}^{N} X_i(k) \tag{16}$$

The position of a hawk in iteration k is denoted as $X_i(k)$, where there are N hawks in total. As the hawk approaches its target prey, convergence must be enhanced, which is why energy equations are employed.

$$E = 2E_0(1 - \frac{k}{T}) \tag{17}$$

E_0 denotes the baseline energy, T the maximum number of iterations, k the current iteration, and E the current energy.

The beginning energy level of the search operation is represented by E_0. T denotes the maximum number of iterations for the search procedure. The current iteration number is kt and the current energy level is represented by E. If the absolute value of E_0 is greater than or equal to one during the search process, the algorithm enters the search phase. If the absolute value of E_0 is less than one, the algorithm enters the exploitation phase.

5.2.2. Exploitation Phase

The Harris hawks launch a surprise attack on the prey they discovered in the previous phase during the exploitation phase. During this phase, the HHO algorithm employs one of four strategies depending on the values of $|E|$ and r. The quantity of energy in the rabbit is represented by $|E|$, and the possibility of the prey escaping is represented by r. A value of r less than 0.5 indicates that the prey successfully escaped, whereas r larger than or equal to 0.5 indicates that the escape was unsuccessful. The Harris hawks have surrounded their victim at this point, and they proceed with either a hard or soft besiege depending on their energy level. When $|E|$ is larger than or equal to 0.5, a light besiege is used, whereas a hard besiege is used.

Soft Besiege

As stated previously, a soft attack occurs when r and $|E|$ is greater than or equal to 0.5. Equations (18) and (19), respectively, present the formulation of soft besiege

$$X(k+1) = \Delta X(k) - E|JX_{ra}(k) - X(k)| \tag{18}$$

$$\delta X(k) = X_{ra}(k) - X(k) \tag{19}$$

The formulation of gentle besiege is represented by the Equations (18) and (19), where $\delta X(k)$ represents the difference between the position vector of the prey and its present location in iteration t. r_5 is a random number within (0, 1), and $J = 2(1 - r_5)$ represents the rabbit's random jump strength throughout the escaping procedure. To simulate the nature of rabbit motions, the J value changes at random during each iteration.

Hard Besiege

When the prey's escape probability r is more than or equal to 0.5 and the prey's energy level $|E|$ is less than 0.5, the hard besiege occurs. In this case, Equation (28) is used to updating the current positions [49].

$$X(k+1) = X_{ra}(k) - E|\delta X(k)| \tag{20}$$

Soft Besiege with Progressive Rapid Dives

Soft attack with progressive quick dives occurs when r is less than 0.5 and $|E|$ is more than or equal to 0.5. To carry out a soft besiege with progressive rapid dives, it is assumed that the Hawks can evaluate (decide) their next move using Equation (21) [49].

$$M = X_{ra}(k) - E|JX_{ra}(k) - X(k)| \tag{21}$$

They are expected to dive based on LF-based patterns using Equation (22):

$$Q = Y + P \times LF(D) \tag{22}$$

where D is the number of dimensions of the problem, P is a random vector of size $1 \cdot D$, and LF is the levy flight function calculated using Equation (23) [49].

$$LF(x) = 0.01 \times \frac{\mu \times \sigma}{|\nu|^{\frac{1}{\beta}}}, \sigma = (\frac{\zeta(1+\beta) \times sin(\frac{\pi\beta}{2})}{\zeta(\frac{1+\beta}{2}) \times \beta \times 2^{\frac{\beta-1}{2}}} \tag{23}$$

where μ and σ are random values ranging from 0 to 1 and β is a constant that is set to 1.5. As a result, the last strategy for adjusting hawk positions during the soft besiege phase can be performed by Equation (24) [49]:

$$X(t+1) = \begin{cases} M & if \quad F(M) < F(X(K)) \\ Q & if \quad F(Q) < F(X(K)) \end{cases} \tag{24}$$

The values of M and Q are found using Equations (21) and (22), respectively [49].

Hard Besiege with Quick Progressive Dives

In the case of a hard besiege with progressive quick dives, the current location is updated using Equation (25) when $r < 0.5$ and $|E| < 0.5$ [49]:

$$X(t+1) = \begin{cases} M' & if \quad F(M') < F(X(K)) \\ Q' & if \quad F(Q') < F(X(K)) \end{cases} \tag{25}$$

where M' and Q' are computed using the following Equations (26) and (27) [49]:

$$M' = X_{ra}(K) - E|JX_{ra}(K) - X_p(K)| \tag{26}$$

$$Q' = Y + P \times LF(D) \tag{27}$$

5.3. Proposed Hybrid Algorithm (HHHOPSO)

Particle Swarm Optimization (PSO) and Harris Hawks Optimization (HHO) are two algorithms that have been combined in the proposed method to optimize maximum power point tracking (MPPT) in a solar-wind system. The selection of these algorithms is based on their distinctive characteristics in addressing optimization problems. HHO draws inspiration from the hierarchical hunting behavior of Harris hawks, while PSO is influenced by the collective behavior of a particle swarm. By leveraging these natural mechanisms, these algorithms offer benefits in exploring and optimizing complex search spaces. In comparison to other optimization techniques, as presented in Table 2, the HHO and PSO algorithms exhibit several advantages. The inclusion of HHO enhances the algorithm's robustness, enabling efficient exploration and avoiding local optima solution. Additionally, Particle Swarm Optimization improves convergence speed, enabling the attainment of the maximum power point more quickly, even in dynamic and changing environmental conditions. Moreover, both HHO and PSO algorithms are renowned for their

global search capabilities, which are crucial for MPPT in the hybrid system characterized by extensive and intricate search spaces.

MPPT presents a multi-modal optimization problem, wherein multiple optimal solutions or local maxima may exist. HHO and PSO algorithms have demonstrated effectiveness in addressing such challenges by maintaining population diversity and exploring various regions in local search space. This capability facilitates the identification of multiple optimal duty cycles for both solar and wind systems, consequently enhancing the overall performance of the hybrid system.

HHO and PSO algorithms offer also more flexibility in terms of tuning and customization parameters. The performance of these algorithms can be improved by adjusting population size, acceleration coefficients, and inertia weight criteria. This allows for adaptation to the specific characteristics and requirements of the MPPT problem in a solar-wind system.

Additionally, HHO and PSO have been widely applied to various optimization problems and have demonstrated success in finding optimal solutions [50–52].

This provides a solid foundation for using the above algorithms for MPPT in a solar-wind system.

By combining the strengths of HHO and PSO, the proposed method aims to achieve robust and efficient MPPT in a solar-wind system, leveraging their global search capabilities and adaptability to changing conditions.

Table 2. MPPT methods benefits and drawbacks.

MPPT Techniques	Benefits	Drawbacks
Perturb & Observe (P&O)	Simplicity and cost-effectiveness.	Oscillations, slow tracking response, and inaccurate tracking under partial shading.
Fuzzy Logic (FL)	Adaptability to varying environmental conditions and robustness in handling noise and partial shading.	Computational complexity depend on the system.
Cuckoo Search Algorithm (CSA)	Global optimization capability, efficient convergence, and robustness.	Computational complexity, tuning sensitivity, lack of standardization, and limited research.
Adaptive Neuro-Fuzzy Inference System (ANFIS)	Adaptability, accuracy, robustness, and flexibility.	Complexity in computing and the implementation process.
Emperor Penguin Optimization algorithm (EPO)	Robustness, potential for global optimization, and efficient searching of the power-voltage curve.	Computational complexity. Requires extensive experimentation and optimization, for parameter tuning.
PSO	Global optimization capability, high efficiency, fast convergence, and robustness to partial shading.	Imbalanced exploration-exploitation and slow adaptation to dynamic conditions.
HHO	Global search capability, efficient convergence, and robustness to local optima.	Ignore previous best positions and requiring parameter tuning.

In this regard, the proposed methodology HHHOPSO-MPPT technique is used to determine the best duty cycle for each SEPIC converter that manages power demand. The fitness function is considered as the output duty cycle. To improve the search process in the proposed methodology, the HHO algorithm with the help of PSO is used. The use of global and local best points in the PSO algorithm is predicted to improve the efficiency of the HHO algorithm in addressing optimization challenges. By optimizing the duty cycle for each converter the power generated by the proposed hybrid energy harvesting system is enhanced.

Below is an explanation of the proposed HHHOPSO algorithm, and Algorithm 2 presents the pseudocode depicting the basic steps in this proposed methodology process.

Algorithm 2 Pseudocode of the proposed methodology

Inputs: The population size n and a maximum number of iterations T_{max}.
Outputs: Save the best Energy and duty cycle
Initialize the HHO and PSO parameters.
Initialize the population of HHO hawks.
Compute fitness function.
Store optimal position and assign fitness function.
while $T < T_{max}$ **do**
    Repeat until Fitness threshold
    Evaluate the fitness
    Update the best positions and fitness values
    Update the positions of the hawks using HHO equations
    Checking the Stopping Criteria
    If condition satisfied, stop the HHO algorithm
    Initialize the population of PSO particles with the optimized positions from HHO.
    Initialize the velocities for each particle
    Repeat until Fitness threshold
    Evaluate the fitness
    Update the best positions and fitness values
    Update the global best position and fitness value
    Update the velocities and positions of the particles using PSO equations
    Checking the Stopping Criteria
    If condition satisfied,
    stop the HHO algorithm
end while stop condition satisfied save the optimal parameter
Return

The HHO and PSO method for MPPT optimization involves several steps.

Step 1: Initially, the parameters of either the photovoltaic or wind turbine system must be initialized.

Step 2: The first step of the exploration process entails implementing HHO. This is achieved by initializing a hawks population n. Additionally, a fitness function is created to evaluate the performance of the MPPT system. In the case of utilizing a photovoltaic (PV) system, the fitness function is represented as $f(n) = MaximizeP_{PV}(d0)$, where $d_{min} \leq d0 \leq d_{max}$ and $V_{pv}min < V_{PV} < V_{pv}max$. On the other hand, in the case of utilizing a wind turbine (WT) system, the fitness function is represented as $f(n) = MaximizeP_{wt}(d1)$, where $d_{min} \leq d1 \leq d_{max}$ and $V_{wt}min < Vwt < V_{wt}max$. It is important to note that the output power from the PV system is represented as P_{PV}, while that of the WT system is represented as P_{wt}. The duty cycle of each SEPIC converter is represented as d0 and d1, respectively. Additionally, the maximum and minimum duty cycles of the DC-DC converter are represented as dmax and dmin. HHO is an optimal search space exploration technique that provides best solutions. Finally, each solution is assessed for its fitness using the aforementioned function.

Step 3: In this step, the optimal solutions derived from the HHO approach are carefully selected. These solutions serve as the initial positions for the PSO algorithm, thereby ensuring the highest level of performance and efficiency.

Step 4: Particle Swarm Optimization (PSO) optimization: the optimal solutions from HHO are used to populate the PSO population. The fitness function for PSO is defined, and the fitness of each particle is evaluated. The positions and velocities of the particles are updated based on their previous positions and velocities, as well as the best solutions determined. The fitness function is used to calculate the fitness of the updated particles. The procedure of updating the locations and velocities of the particles is repeated until convergence is reached or a halting requirement is met.

Step 5: Following each PSO iteration, the Harris hawks' positions are updated using the best PSO solutions. The Harris hawks are permitted to adjust their positions based on

the information acquired by PSO, allowing them to explore previously unexplored regions of the search space.

Step 6: Steps 5–6 must be repeated until the termination criteria are met.

Step 7: The HHHOPSO algorithm extracts the maximum power of the PV panels or rectifier.

Step 8: Send the duty cycle to the SEPIC converter.

This proposed methodology is used to select the optimal duty cycles of each SEPIC converters at the maximum power of the PV panels and the rectifier. This results in improved power generation performance. The proposed method may improve the efficiency and stability of hybrid renewable energy systems, which are becoming increasingly important renewable energy sources.

6. IoT Devices and Network Lifetime

IoT sensors play a critical role in enabling the accumulation and analysis of data for various applications, such as environmental monitoring, security surveillance, and healthcare. In this context, to ensure proper operation and optimal performance, it is essential to consider their specific working voltage range and power requirements. The effective voltage varies depending on the sensor type and intended application from millivolts to a few volts. This low voltage is necessary to conserve energy and extend the sensor's battery lifespan, considering that most IoT sensors require power for a brief period with an extended period of inactivity. Furthermore, lower power consumption is particularly essential in IoT applications where a large number of electronic devices are typically employed. In such systems powered by energy harvesters, the voltage level required for a launch often determines the mechanisms used.

In our work, we set the functional voltage and power requirements for some applied IoT sensors based on the manufacturer specification sheets. To calculate the initial energy of each IoT node, we used alkaline batteries with a voltage of 1.5 V, AA dimensions, and a 1000 mAh capacity. Since each node has two AA-size batteries, the initial energy of one node with two batteries is 7200 J. In our study, we created a network of 500 sensor nodes, having the same initial energy. Thus, the resulting energy amounts of the entire network is 3,600,000 J.

The IoT network lifetime refers to the duration in which the network remains operational before becoming non-operational. It depends on the data gathering and measurement activities. The formula to calculate the network lifetime $E_{(IoT)}$ is as follows:

$$E_{(IoT)} = \frac{(E_o - E_{(WE)})}{(P_C + P_{(Rate)}) \times E_s} \tag{28}$$

Here, E_o represents the initial energy of the network, $E_{(WE)}$ and E_s are the wasted energy and the energy consumed, respectively, P_C refers to the overall power consumed and $P_{(Rate)}$ denotes the rate at which packets are received.

Every sensor node consists of a transmitter and a receiver. The first one provides energy to both radio electronics and power amplifier, whereas the receiver provides energy to the radio electronics.

This energy transfer process takes into account the multipath fading model. When compared to the defined threshold d_0, the distance d between the transmitter and receiver increases and determines the dominant energy dissipation mechanism.

The energy dissipation encountered in free space is denoted as d^2. The energy dissipation relating to the multipath is then denoted by d^4. The energy dissipation model during the k-bit data packet transmission is represented in Equation (29)

$$E_{TX}(K,d)\begin{cases} = E_{elec} \times K + \varepsilon_{fs} \times K \times d^2 & if \;\; d < d_0 \\ = E_{elec} \times K + \varepsilon_{mp} \times K \times d^4 & if \;\; d \geq d_0 \end{cases} \tag{29}$$

where the energy dissipated by the electronic circuits is denoted as E_{elec}. Free space amplifier energy ε_{fs}, and multipath amplifier energy ε_{mp}, contribute to energy dissipation. The threshold distance, d_0, is determined by: $d_0 = \sqrt{\frac{\varepsilon_{fs}}{\varepsilon_{mp}}}$.

The energy dissipation experienced by a sensor node when receiving a k-bit data packet is described by Equation (30).

$$E_{RX}(K) = E_{elec} \times K \tag{30}$$

7. Results and Discussion

This section validates and justifies the proposed methodology. Our study was carried out on the MATLAB/Simulink environment. To improve the lifetime of IoT networks, we propose using a hybrid solar-wind turbine (PV-WT) system. We constructed a network of 500 sensor nodes with identical initial and maximum energy capacities.

Figures 4 and 5 illustrate the subsystems of the solar and wind energy harvester. The primary main objective of this research is to optimize power extraction from the hybrid system. To accomplish this, the HHHOPSO algorithm is used, aiming to maximize the overall power generation.

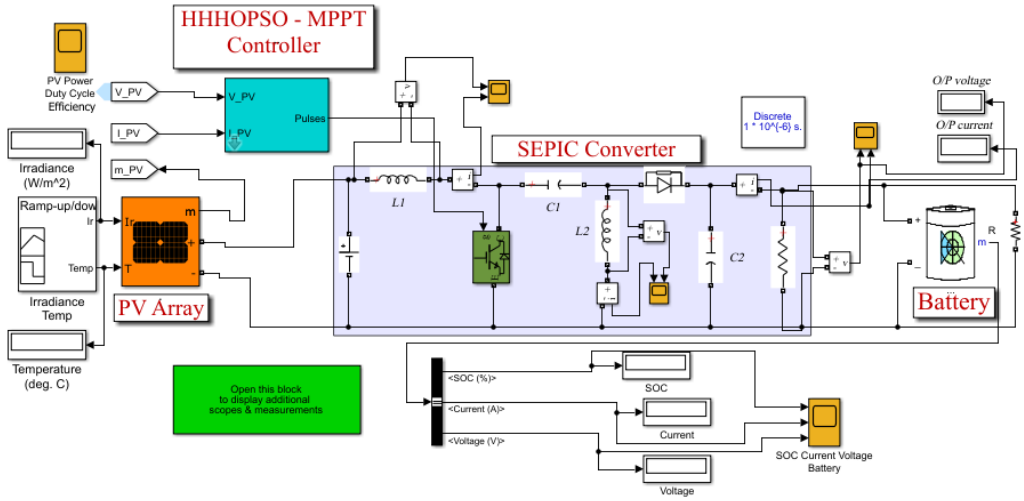

Figure 4. Simulink model of the solar system using the HHHOPSO MPPT technique.

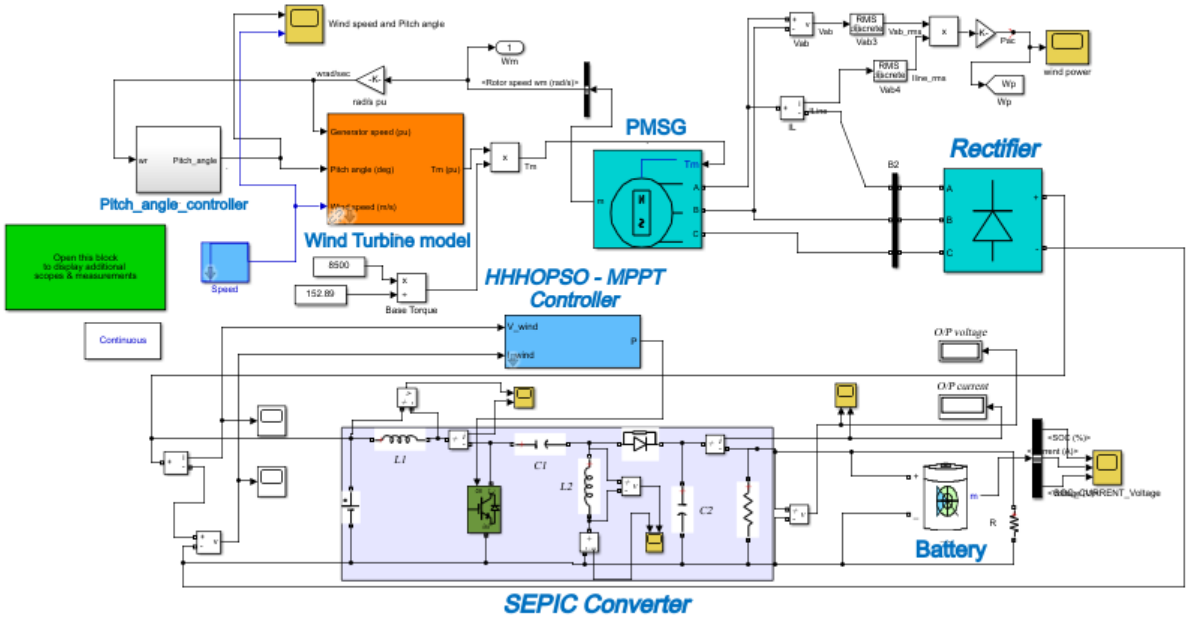

Figure 5. Simulink diagram of the wind energy system.

Table 3 lists the essential parameters of the PV module under standard conditions (1000 W/m^2 at 25 °C), wind turbines, and battery characteristics.

Table 3. Simulation parameters.

Method	Description	Parameters
PV	Max. PV Current	600 mA
	Max. PV voltage	4 V
Wind	Wind speed	12 m/s
	Wind power	245 mW
Battery	Battery Voltage	3.7 V
	Battery type	lithium-ion
	Battery capacity	730 mAh
IoT-WSN Load Model	R	10 Ω

The PSO technique involves the creation of an initial population with the assistance of the HHO algorithm. The proposed methodology is designed to extract maximum power from the system and determine the optimal duty cycle of each DC-DC SEPIC converter. The hybrid PV-WT approach is used in this proposed methodology for charging the IoT nodes and enhance the network's lifetime.

The power generated by the PV system is affected by temperature and irradiance, as shown in Figure 6. Figure 7 shows the PV system's output of voltage and current. In this system, the PV system generates power is based on a fixed irradiance of 1000 W/m^2 and a temperature of 25 °C. The PV system produces a voltage of 4.7 V and a current of 0.6 A. The generated power from the PV system is used to charge a storage battery.

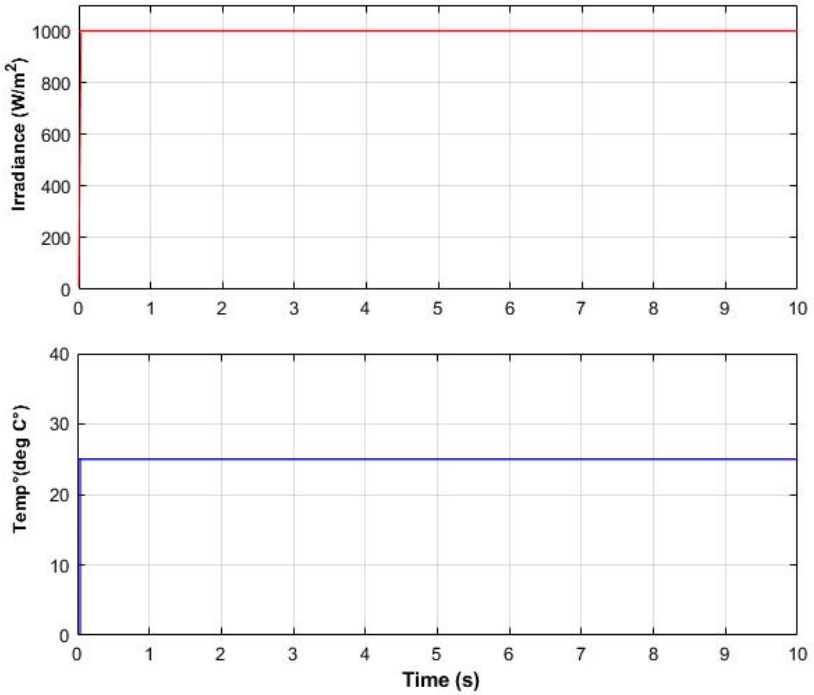

Figure 6. Stable irradiance and temperature of PV system.

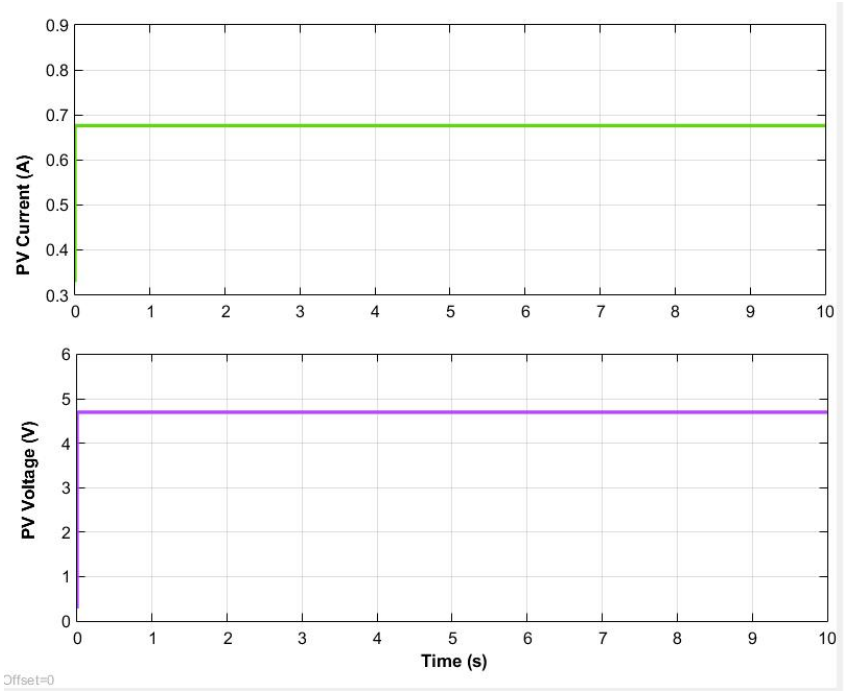

Figure 7. PV voltage and current.

In the proposed methodology, the utilization of wind energy is also taken into account for the purpose of charging IoT nodes. Wind speed of 12 m/s is considered for wind power generation, as depicted in Figure 8. The wind power generated is quantified at 958 mW, as shown in Figure 9.

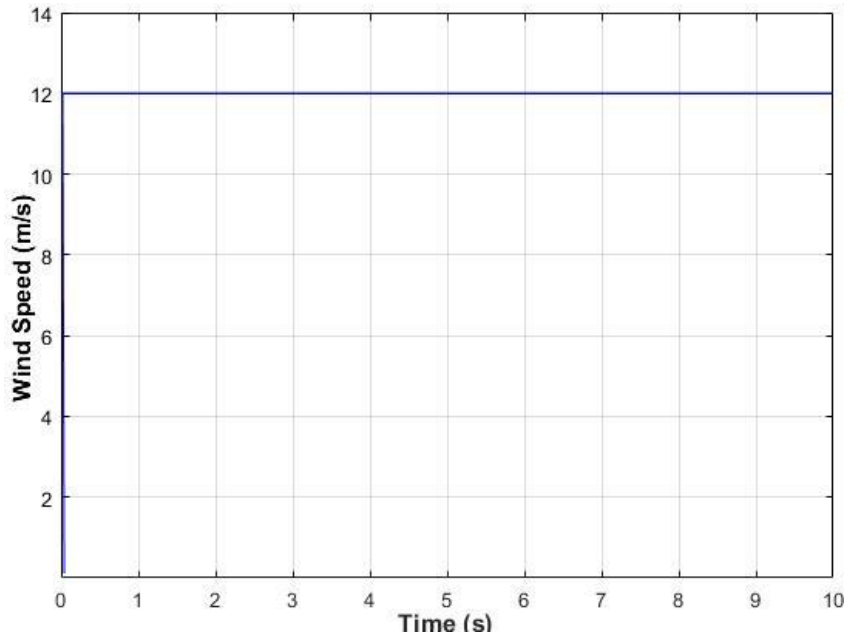

Figure 8. Wind speed vs. time.

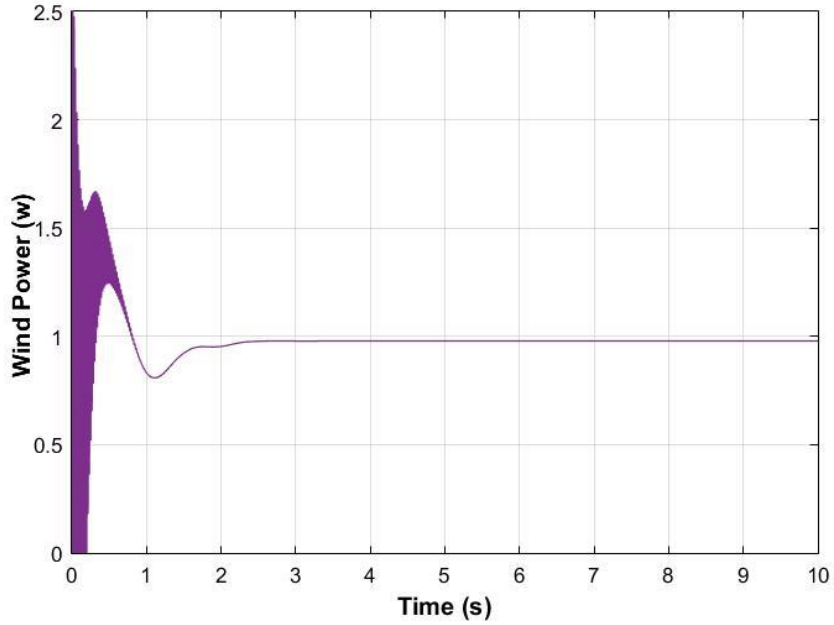

Figure 9. Wind power generation.

Additionally, the power generated by PV is illustrated in Figure 10, with a value of 2.4 W.

Figure 11 demonstrate that the MPPT algorithm has efficiently tracked close to the maximum power from both the PV array and the WT. The tracking time of the proposed MPPT in the PV system and wind system is less than 0.2 s, with the highest tracking efficiency of 98.24% achieved at a solar irradiance of 1000 W/m^2 and wind speed of 12 m/s.

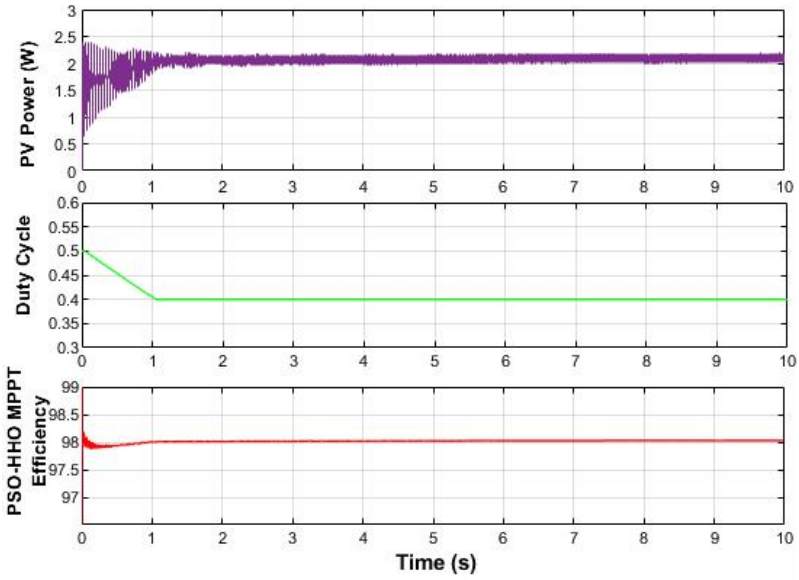

Figure 10. Tracking performance of the HHHOPSO-MPPT algorithm in a PV system.

Based on the amount of current and voltage coming from the PV panel and rectifier, the HHHOPSO MPPT controller generates the optimum duty cycles that are used to activate each SEPIC converter. The SEPIC converter controls how much voltage is sent to the battery before sending the collected voltage. Figure 12 depicts the DC bus voltage of 4.5 V for the proposed design, which needs to be maintained at a constant level for efficient operation. To combine the outputs of solar and wind sources in a DC bus, both sources

must be operating at the same voltage level. A DC-DC SEPIC converter can step up each source's voltage to meet the DC bus's voltage level.

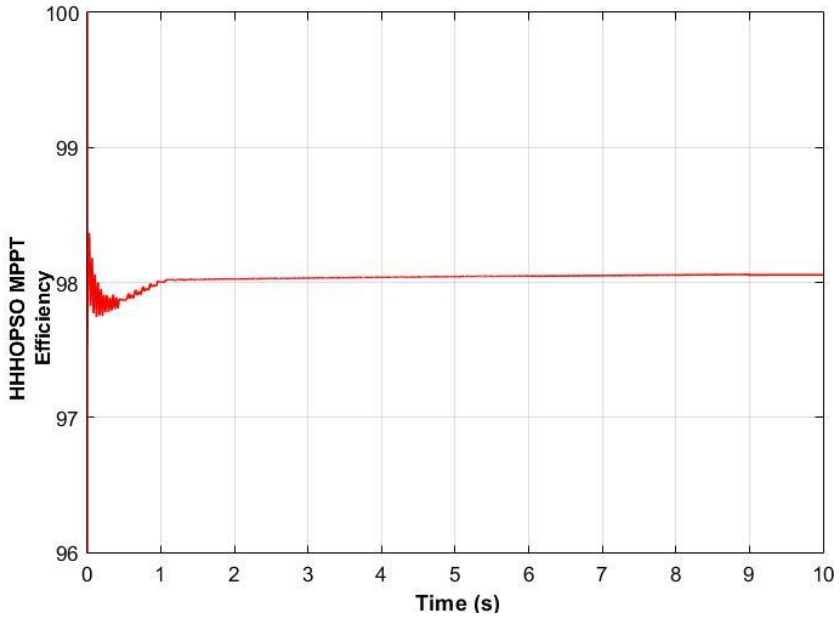

Figure 11. Efficiency of the proposed method.

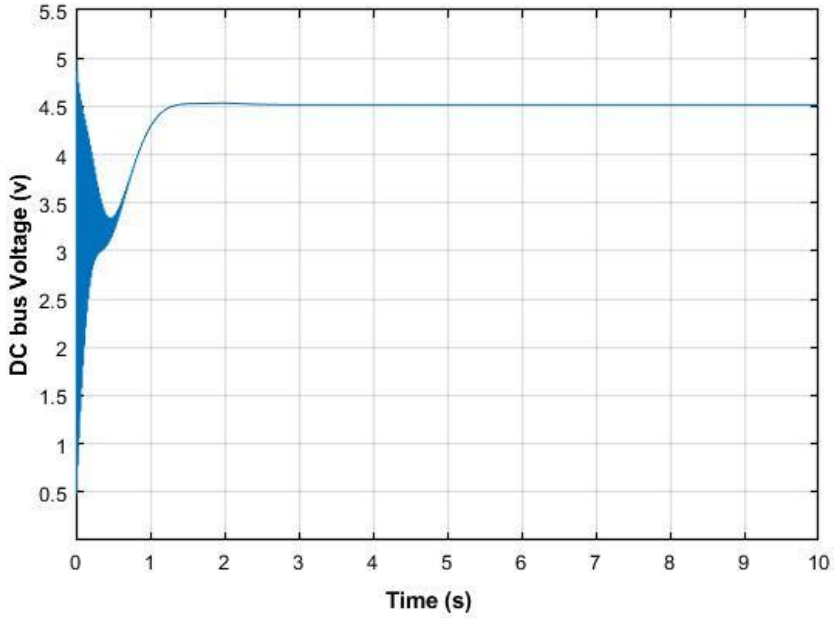

Figure 12. DC link voltage vs. time.

Figures 13–18 show the comparison study of the proposed technique. The performance of a hybrid solar-wind energy harvesting battery charger is compared using the proposed methodology with the conventional methods namely PWM and P&O-MPPT. The performance is evaluated in terms of the battery state of charge (SoC), voltage, current and efficiency.

Figure 13 shows the results for the PWM control technique. The voltage ranges from 0 to 2.8 V, the current ranges from 0 to −1.3 A, and the battery's SoC ranges from 50% to 51.6% over a 10 s simulation.

Figure 14 displays the results for the P&O-MPPT controller. The voltage ranges from 0 to 4 V, the current ranges from 0 to −2 A, and the battery's SoC ranges from 50% to 56.14% over the same simulation time.

Figure 15 presents the results of the proposed technique. The voltage ranges from 0 to 4.8 V, the current ranges from 0 to −1 A, and the battery's SoC ranges from 50% to 66%. During charging, the battery current is negative, indicating the oxidation process occurring within the electrochemical cells.

Additionally, the comparative study of the battery performance among different control techniques is depicted in Figures 16–18 within an increased simulation time of 100 s. Figure 16 shows the results of the PWM controller, Figure 17 represents the P&O-MPPT controller, and Figure 18 presents the performance of our proposed HHHOPSO-MPPT system.

In terms of battery performance, the HHHOPSO-MPPT system outperforms the other two controllers. It achieves 100% state of charge (SoC) in the shortest simulation time of 88 s. On the other hand, the P&O-MPPT and PWM systems take longer to reach 91% and 82% SoC, respectively, within a simulation time of 100 s.

Figure 18 illustrates the results obtained with our proposed method for an extended simulation time of 100 s. The voltage ranges from 0 to 4.8 volts, while the current ranges from 0 to −1 A. Both the current and voltage exhibit constant values throughout the simulation.

Comparing these results with those presented in Figure 16 for the PWM controller and Figure 17 for the MPPT-P&O controller, notable differences in voltage and current ranges can be observed. In Figure 16, the voltage ranges from 0 to 2.8 V, and the current ranges from 0 to −1.3 A. In Figure 17, the voltage ranges from 0 to 3.8 V, and the current ranges from 0 to −2 A.

These figures provide insights into the performance differences among the control techniques, highlighting the improved battery SoC and voltage ranges achieved by the proposed technique compared to conventional methods.

Choosing an appropriate load resistance that balances power requirements, discharge rate, and overall system efficiency is crucial. Therefore, we conducted an evaluation of battery performance under varying loads. Specifically, we ran tests with load variations of 2 ohms, 10 ohms and 30 ohms. The voltage and current variations of battery for the three load values are depicted in the following Figure 19.

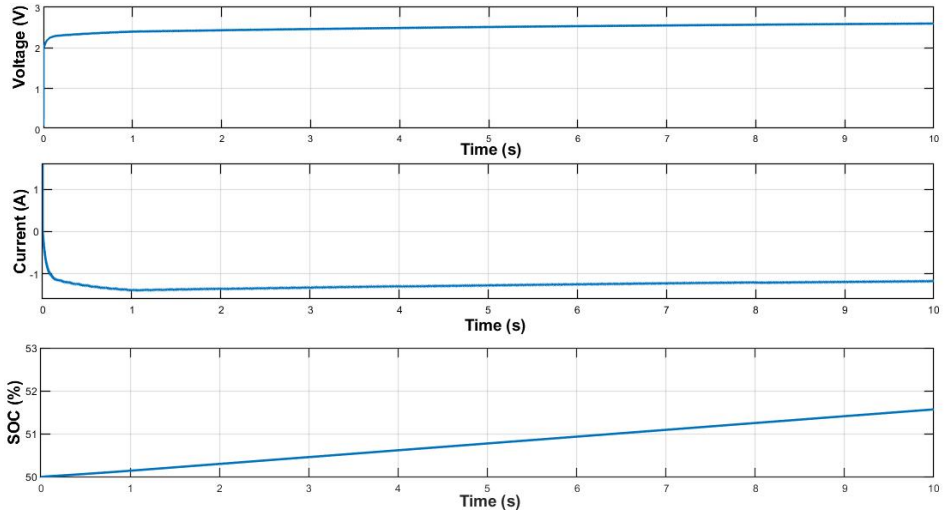

Figure 13. Battery performance using PWM controller for 10 s.

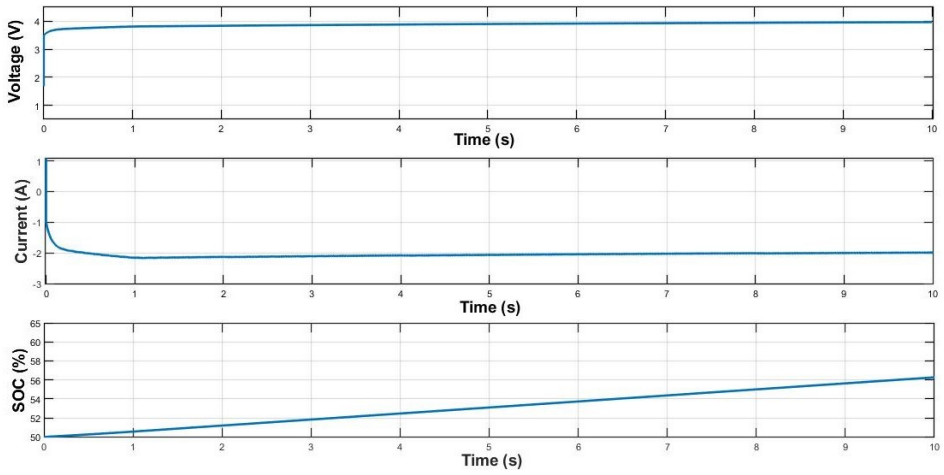

Figure 14. Battery performance using MPPT-P&O controller for 10 s.

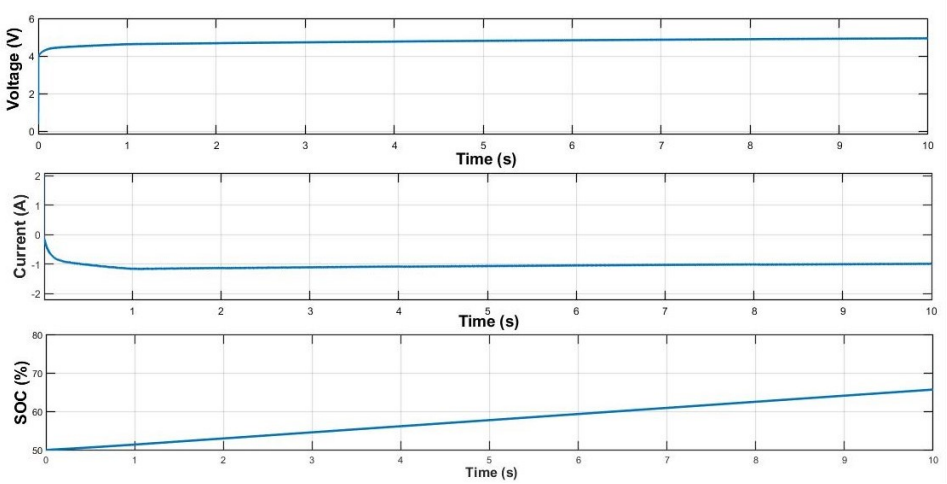

Figure 15. Battery performance using HHHOPSO-MPPT controller for 10 s.

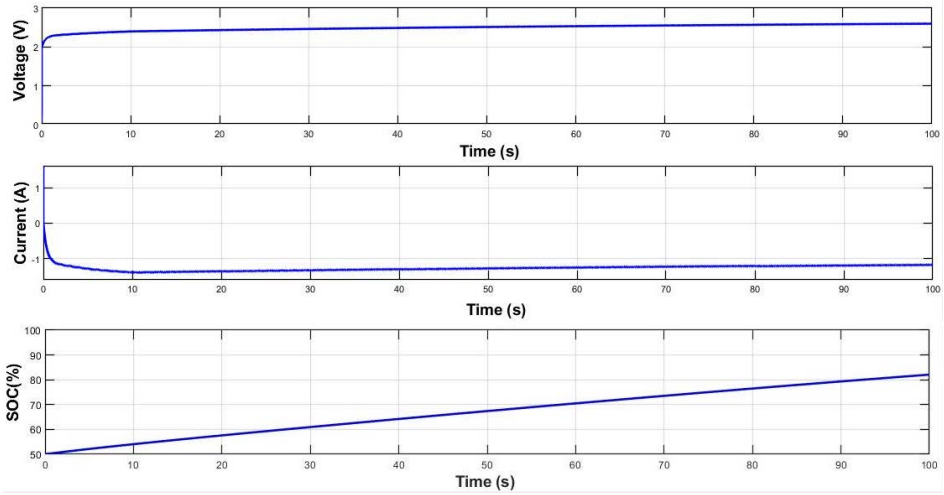

Figure 16. Battery performance using PWM controller for 100 s.

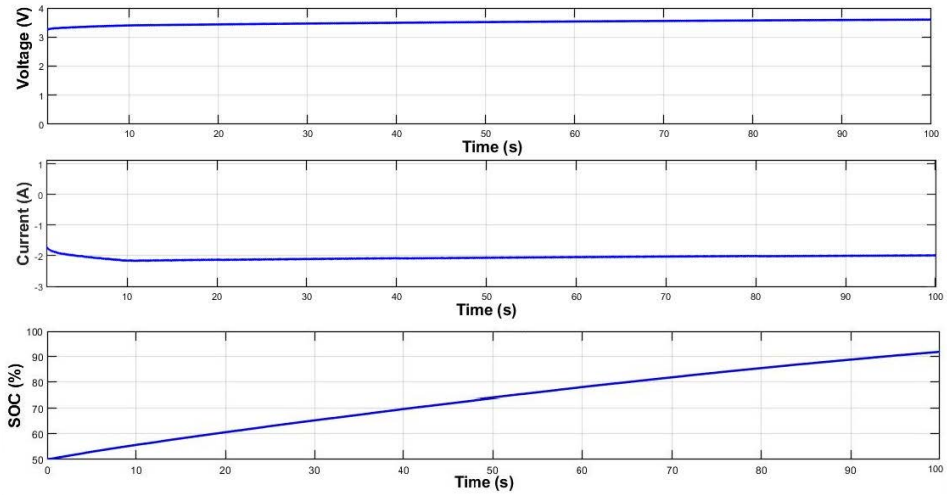

Figure 17. Battery performance using MPPT-P&O controller for 100 s.

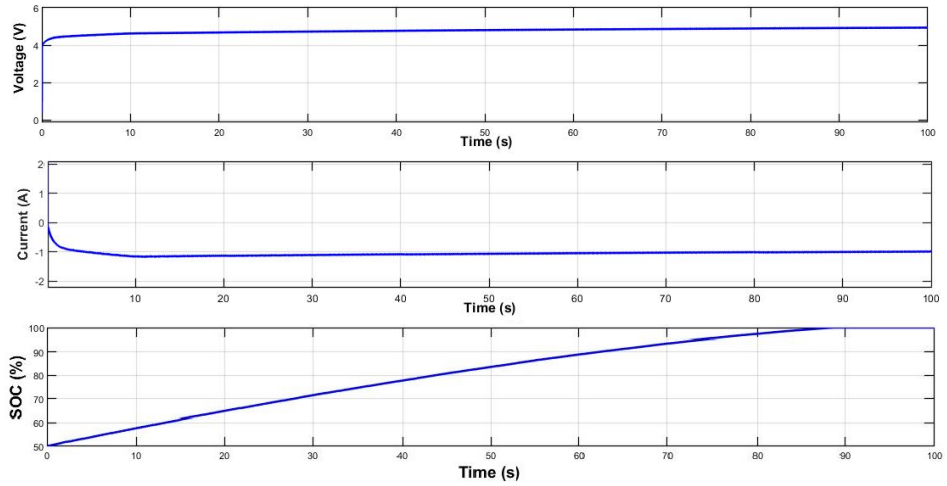

Figure 18. Battery performance using HHHOPSO-MPPT controller for 100 s.

Figure 19a shows the results for the load resistance R = 2 ohms. The voltage varies from 0 to 8 V and whereas the current range from 0 to −4 A. When the load resistance is very low, the battery is subject to a heavy current draw, potentially leading to a significant drop in voltage.

Figure 19b illustrates the outcomes for the load resistance R = 10 ohms. The voltage varies from 0 to 4.8 V, while the current ranges from 0 to −1 A. Increasing the load resistance to 10 ohms would limit the current flowing through the circuit. As a result, the voltage across the battery may remain relatively stable compared to the case with a lower resistance.

In Figure 19c, the results for the load resistance R = 30 ohms are depicted. The voltage ranges from 4 to 2.3 V, while the current ranges from −1 to 2.2 A. When increasing the load resistance to 30 ohms would further restrict the current flowing through the circuit. Consequently, the voltage across the battery may experience drop compared to the previous scenarios.

Thus, it is obvious that changing the load resistance has a direct impact on battery performance, affecting the discharge rate, voltage stability, and overall efficiency. Lower load resistance leads to higher discharge rates and increased power consumption. However, higher load resistance reduces the discharge rate, resulting in lower power consumption.

We can conclude that the system efficiency is optimized when the load resistance matches the internal resistance of the battery. This ensures efficient power transfer without significant losses. Balancing load resistance with system requirements is essential for achieving optimal battery performance and maximizing overall system effectiveness.

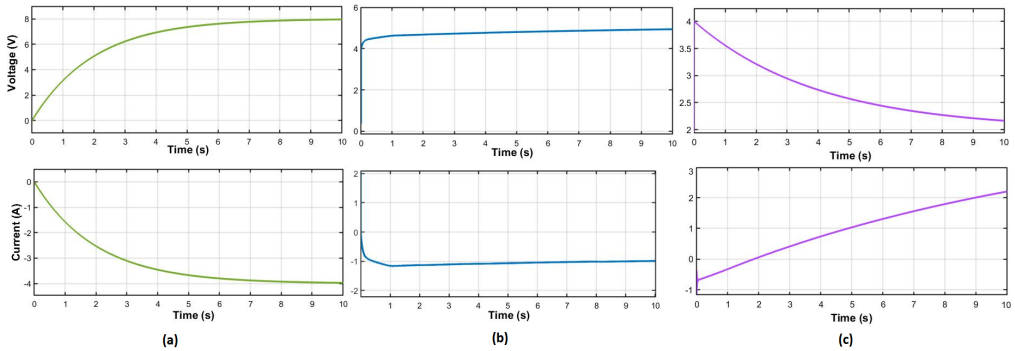

Figure 19. Effect of load resistance on battery voltage and current. (**a**) R = 2 ohms, (**b**) R = 10 ohms, (**c**) R = 30 ohms.

Figure 20 compares the efficiency of the proposed hybrid MPPT controller with an existing controller algorithm. The results indicate that the proposed technique achieved an efficiency of 98.24%, while the existing PWM and MPPT-P&O controllers had efficiencies of 88.72% and 96.6%, respectively. The results indicate that the proposed technique exhibits higher efficiency compared to the other two methods.

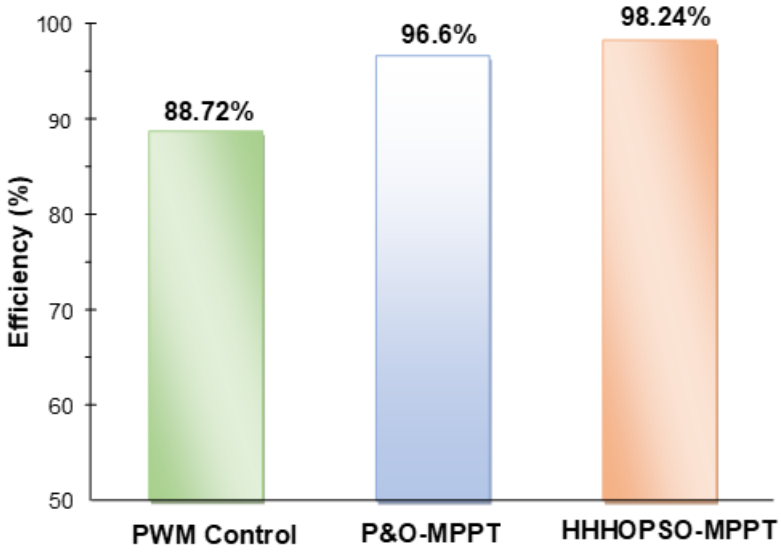

Figure 20. Comparison of PWM, P&O-MPPT and proposed HHHOPSO-MPPT harvesting system efficiency.

Table 4 shows the simulation results comparing PWM, P&O-MPPT, and HHHOPSO-MPPT control algorithms for solar-wind energy harvesting system. This table presents the average power, tracking time, and tracking efficiency for each algorithm. The results demonstrate that the proposed technique achieves an average traking time of 0.1751, faster than the two conventional algorithms. Moreover, it delivers higher average power and improved efficiency, with an increase of 9.68% and 1.8% compared to PWM and P&O-MPPT, respectively.

Table 4. Comparative analysis of MPPT method.

Methods	Average Power	Tracking Time (s)	Harvester System Efficiency (%)
PWM	2.67 W	2.016 s	88.72%
P&O	2.94 W	0.1876 s	96.6%
Proposed	3.3 W	0.1751 s	98.24%

Figure 21 describes the influence of the energy harvesting mechanism on extending the lifetime of the network. A comparison of network lifetimes is conducted between using or not a hybrid energy harvesting system. The network lifespan is presently quite limited, as demonstrated by the 20-day lifespan in the absence of energy harvesting. However, when a hybrid energy harvesting approach is employed and the MPPT is appropriately optimized, the network lifecycle is substantially extended to 122 days. This is accomplished by achieving the maximum power output from solar, wind, or both at the same time. Therefore, the integration of energy harvesting mechanisms is critical for maintaining system operation and enhancing its longevity.

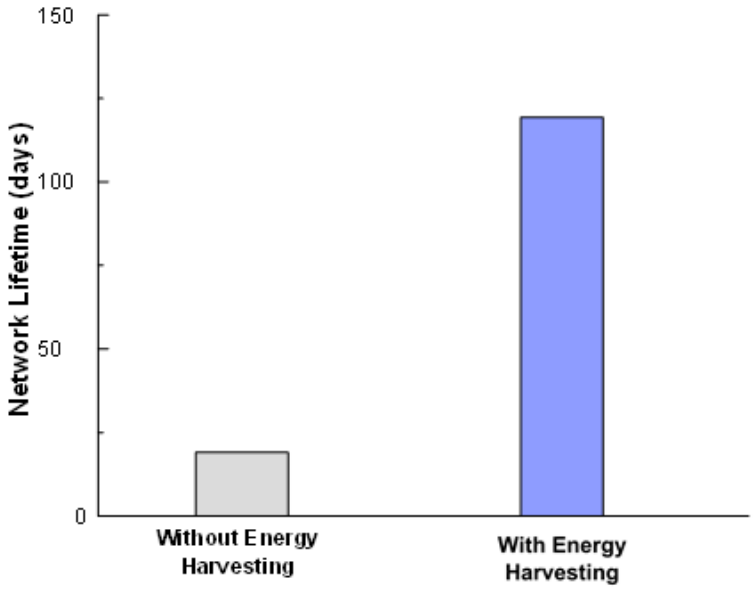

Figure 21. IoT network lifetime comparison before and after energy harvesting.

A comparison was made of various recently published energy-harvesting systems for WSNs or IoT as shown in Table 5. Similarly, in Refs. [17,31], other researchers have proposed their own energy harvesting models with different simulation parameters. The results demonstrate that the proposed energy-harvesting system achieved the highest efficiency rate of up to 98.24% compared to other simulation works.

Table 5. An overview of different energy harvesting systems used in IoT networks.

Author&Year	Energy Sources	Converter Type	MPPT	Peak Efficiency (ν)
Sharma, H., et al. [31], 2018	Solar	Buck Converter	PWM & MPPT both	96.06%
Saraereh, O. A., et al. [53], 2020	TEG-RF	Boost converter	No	Not Reported
Tran, Hoang T., et al. [54], 2022	Solar-RF	Boost converter	P&O-MPPT	Not Reported
P. Gupta et al. [17], 2022	Solar	SEPIC Boost converter	MPPT-EPO	98%
Xiao, Heng, et al. [55], 2023	PV-TEG	unidirectional DC/DC converter	Not Reported	Not Reported
Proposed methodology	Solar PV-wind	SEPIC Buck-boost DC/DC converter	HHHOPSO-MPPT	98.24%

8. Conclusions

This study presents the design and analysis of a hybrid solar-wind system equipped with a SEPIC converter. Our approach combines HHO and PSO optimization algorithms to extract maximum power and enhance the lifetime of IoT devices. The primary objective of the proposed methodology is to maximize power generation from both solar and wind systems. Thus, to evaluate the performance of the suggested method, the MATLAB/Simulink

platform is used, and a comparison is made with conventional techniques such as PWM and MPPT-P&O. The analysis focuses on key parameters such as battery current, voltage, state of charge (SoC), IoT network lifetime, and efficiency. Switches were assessed for the following simulation periods: 0 to 10 s and 0 to 100 s.

Hence, the battery power is significantly increased by optimizing the MPPT algorithm to harness more power from both the solar and wind energy harvesting systems. Furthermore, the overall efficiency is calculated by considering the efficiencies of the SEPIC converter and HHHOPSO-MPPT for both subsystems. The simulation results demonstrate that our proposed methodology achieves an impressive overall efficiency of 98.24%.

This work suggests several potential future research directions. These include integrating new energy storage systems, implementing real-time monitoring, control, conducting cost and economic analysis. Obviously, these areas will mainly enhance the efficiency, reliability, and economic viability of hybrid solar-wind systems in IoT applications and renewable energy systems.

Author Contributions: Conceptualization, S.R., A.Z., J.L. and H.D.; methodology, S.R., A.Z., J.L. and H.D.; software, S.R., A.Z., J.L. and H.D.; validation, S.R., A.Z., J.L. and H.D.; formal analysis, S.R., A.Z., J.L. and H.D.; investigation, S.R. and J.L.; resources, S.R., A.Z., J.L. and H.D.; data curation, S.R., A.Z., J.L. and H.D.; writing—original draft preparation, S.R., A.Z., J.L. and H.D.; writing—review and editing, S.R., A.Z., J.L. and H.D.; visualization, S.R.; supervision, A.Z., J.L. and H.D.; project administration, A.Z., J.L. and H.D. All authors have read and agreed to the published version of the manuscript.

Funding: This research received no external funding.

Institutional Review Board Statement: Not applicable.

Informed Consent Statement: Not applicable.

Data Availability Statement: For Wind system: http://www.solar-i.com/S&Y/wssen.htm.

Conflicts of Interest: The authors declare no conflict of interest.

References

1. Zhang, D.G.; Wu, H.; Zhao, P.Z.; Liu, X.h.; Cui, Y.Y.; Chen, L.; Zhang, T. New approach of multi-path reliable transmission for marginal wireless sensor network. *Wirel. Netw.* **2020**, *26*, 1503–1517. [CrossRef]
2. Shafiq, M.; Tian, Z.; Bashir, A.K.; Du, X.; Guizani, M. IoT malicious traffic identification using wrapper-based feature selection mechanisms. *Comput. Secur.* **2020**, *94*, 101863. [CrossRef]
3. Yu, X.; Yang, X.; Tan, Q.; Shan, C.; Lv, Z. An edge computing based anomaly detection method in IoT industrial sustainability. *Appl. Soft Comput.* **2022**, *128*, 109486. [CrossRef]
4. Yazici, M.S.; Yavasoglu, H.A.; Eroglu, M. A mobile off-grid platform powered with photovoltaic/wind/battery/fuel cell hybrid power systems. *Int. J. Hydrogen Energy* **2013**, *38*, 11639–11645. [CrossRef]
5. Muñoz-Palomeque, E.; Sierra-García, J.E.; Santos, M. Wind turbine maximum power point tracking control based on unsupervised neural networks. *J. Comput. Des. Eng.* **2023**, *10*, 108–121. [CrossRef]
6. Khan, M.J.; Mathew, L. Comparative study of maximum power point tracking techniques for hybrid renewable energy system. *Int. J. Electron.* **2019**, *106*, 1216–1228. [CrossRef]
7. Vasant, L.G.; Pawar, V. Solar-wind hybrid energy system using MPPT. In Proceedings of the 2017 International Conference on Intelligent Computing and Control Systems (ICICCS), Madurai, India, 15–16 June 2017; pp. 595–597. [CrossRef]
8. Rezkallah, M.; Hamadi, A.; Chandra, A.; Singh, B. Design and implementation of active power control with improved P&O method for wind-PV-battery-based standalone generation system. *IEEE Trans. Ind. Electron.* **2017**, *65*, 5590–5600. [CrossRef]
9. Fathabadi, H. Novel standalone hybrid solar/wind/fuel cell power generation system for remote areas. *Sol. Energy* **2017**, *146*, 30–43. [CrossRef]
10. Ram, J.P.; Rajasekar, N.; Miyatake, M. Design and overview of maximum power point tracking techniques in wind and solar photovoltaic systems: A review. *Renew. Sustain. Energy Rev.* **2017**, *73*, 1138–1159. [CrossRef]
11. Vardia, M.; Priyadarshi, N.; Ali, I.; Azam, F.; Bhoi, A.K. Maximum power point tracking for wind energy conversion system. In *Advances in Greener Energy Technologies*; Springer: Singapore, 2020; pp. 631–640. [CrossRef]
12. Qais, M.H.; Hasanien, H.M.; Alghuwainem, S. Enhanced whale optimization algorithm for maximum power point tracking of variable-speed wind generators. *Appl. Soft Comput.* **2020**, *86*, 105937. [CrossRef]
13. Kumar, G.A. Optimal power point tracking of solar and wind energy in a hybrid wind solar energy system. *Int. J. Energy Environ. Eng.* **2022**, *13*, 77–103. [CrossRef]

14. Mokhtari, Y.; Rekioua, D. High performance of maximum power point tracking using ant colony algorithm in wind turbine. *Renew. Energy* **2018**, *126*, 1055–1063. [CrossRef]
15. Mahdi, A.; Mahamad, A.; Saon, S.; Tuwoso, T.; Elmunsyah, H.; Mudjanarko, S. Maximum power point tracking using perturb and observe, fuzzy logic and ANFIS. *SN Appl. Sci.* **2020**, *2*, 1–9. [CrossRef]
16. Dhanunjaya, V.; Vijaya Bhaskar Reddy, K.; Vijaya Kumar, S.; Venkata Kishore, P. PV-WIND Hybrid System Based Cuckoo Search Maximum Power Point Tracking Algorithm. In *Innovations in Electrical and Electronic Engineering: Proceedings of ICEEE 2022, Volume 1*; Springer: Berlin/Heidelberg, Germany, 2022; pp. 203–214. [CrossRef]
17. Gupta, P.; Tripathi, S.; Singh, S.; Gupta, V. MPPT-EPO optimized solar energy harvesting for maximizing the WSN lifetime. *Peer-Peer Netw. Appl.* **2023**, *16*, 347–357. [CrossRef]
18. Hai, T.; Zhou, J.; Dadfar, S. A novel intelligent method to increase accuracy of hybrid photovoltaic-wind system-based MPPT and pitch angle controller. *Soft Comput.* **2023**, *27*, 7401–7418. [CrossRef]
19. Aloo, L.A.; Kihato, P.K.; Kamau, S.I.; Orenge, R.S. Modeling and control of a photovoltaic-wind hybrid microgrid system using GA-ANFIS. *Heliyon* **2023**, *9*, e14678. [CrossRef]
20. Renjith, A.; Selvam, P. Efficient maximum power tracking technique in grid connected PV-wind system. *Electr. Power Syst. Res.* **2023**, *214*, 108955. [CrossRef]
21. Elmetwaly, A.H.; Younis, R.A.; Abdelsalam, A.A.; Omar, A.I.; Mahmoud, M.M.; Alsaif, F.; El-Shahat, A.; Saad, M.A. Modeling, Simulation, and Experimental Validation of a Novel MPPT for Hybrid Renewable Sources Integrated with UPQC: An Application of Jellyfish Search Optimizer. *Sustainability* **2023**, *15*, 5209. [CrossRef]
22. Chamanian, S.; Baghaee, S.; Ulusan, H.; Zorlu, Ö.; Külah, H.; Uysal-Biyikoglu, E. Powering-up wireless sensor nodes utilizing rechargeable batteries and an electromagnetic vibration energy harvesting system. *Energies* **2014**, *7*, 6323–6339. [CrossRef]
23. Kamalinejad, P.; Mahapatra, C.; Sheng, Z.; Mirabbasi, S.; Leung, V.C.; Guan, Y.L. Wireless energy harvesting for the Internet of Things. *IEEE Commun. Mag.* **2015**, *53*, 102–108. [CrossRef]
24. Annapureddy, V.; Na, S.M.; Hwang, G.T.; Kang, M.G.; Sriramdas, R.; Palneedi, H.; Yoon, W.H.; Hahn, B.D.; Kim, J.W.; Ahn, C.W.; et al. Exceeding milli-watt powering magneto-mechano-electric generator for standalone-powered electronics. *Energy Environ. Sci.* **2018**, *11*, 818–829. [CrossRef]
25. Williams, A.J.; Torquato, M.F.; Cameron, I.M.; Fahmy, A.A.; Sienz, J. Survey of energy harvesting technologies for wireless sensor networks. *IEEE Access* **2021**, *9*, 77493–77510. [CrossRef]
26. Sudevalayam, S.; Kulkarni, P. Energy harvesting sensor nodes: Survey and implications. *IEEE Commun. Surv. Tutor.* **2010**, *13*, 443–461. [CrossRef]
27. Atallah, R.; Khabbaz, M.; Assi, C. Energy harvesting in vehicular networks: A contemporary survey. *IEEE Wirel. Commun.* **2016**, *23*, 70–77. [CrossRef]
28. Wang, W.S.; O'Donnell, T.; Ribetto, L.; O'Flynn, B.; Hayes, M.; O'Mathuna, C. Energy harvesting embedded wireless sensor system for building environment applications. In Proceedings of the 2009 1st International Conference on Wireless Communication, Vehicular Technology, Information Theory and Aerospace & Electronic Systems Technology, Aalborg, Denmark, 17–20 May 2009; pp. 36–41. [CrossRef]
29. Li, Y.; Shi, R. An intelligent solar energy-harvesting system for wireless sensor networks. *EURASIP J. Wirel. Commun. Netw.* **2015**, *2015*, 179. [CrossRef]
30. Samijayani, O.N.; Firdaus, H.; Mujadin, A. Solar energy harvesting for wireless sensor networks node. In Proceedings of the 2017 International Symposium on Electronics and Smart Devices (ISESD), Yogyakarta, Indonesia, 17–19 October 2017; pp. 30–33. [CrossRef]
31. Sharma, H.; Haque, A.; Jaffery, Z.A. Modeling and optimisation of a solar energy harvesting system for wireless sensor network nodes. *J. Sens. Actuator Netw.* **2018**, *7*, 40. [CrossRef]
32. Saxena, M.; Dutta, S. Improved the efficiency of IoT in agriculture by introduction optimum energy harvesting in WSN. In Proceedings of the 2020 International Conference on Innovative Trends in Information Technology (ICITIIT), Kottayam, India, 13–14 February 2020; pp. 1–5. [CrossRef]
33. Zhao, P. Energy Harvesting Techniques for Autonomous WSNs/RFID with a Focus on RF Energy Harvesting. 2012. Available online: https://tuprints.ulb.tu-darmstadt.de/id/eprint/3102 (accessed on 19 June 2023).
34. Toh, W.Y.; Tan, Y.K.; Koh, W.S.; Siek, L. Autonomous wearable sensor nodes with flexible energy harvesting. *IEEE Sens. J.* **2014**, *14*, 2299–2306. [CrossRef]
35. Lloret, J.; Garcia, M.; Catala, A.; Rodrigues, J.J. A group-based wireless body sensors network using energy harvesting for soccer team monitoring. *Int. J. Sens. Netw.* **2016**, *21*, 208–225. [CrossRef]
36. Park, J.W.; Jung, H.J.; Jo, H.; Jang, S.; Spencer, B.F., Jr. Feasibility study of wind generator for smart wireless sensor node in cable-stayed bridge. In Proceedings of the Sensors and Smart Structures Technologies for Civil, Mechanical, and Aerospace Systems 2010, San Diego, CA, USA, 7–11 March 2010; Volume 7647, pp. 1241–1248. [CrossRef]
37. Tan, Y.K.; Panda, S.K. Self-autonomous wireless sensor nodes with wind energy harvesting for remote sensing of wind-driven wildfire spread. *IEEE Trans. Instrum. Meas.* **2011**, *60*, 1367–1377. [CrossRef]
38. Weimer, M.A.; Paing, T.S.; Zane, R.A. Remote area wind energy harvesting for low-power autonomous sensors. In Proceedings of the 2006 37th IEEE Power Electronics Specialists Conference, Jeju, Republic of Korea, 18–22 June 2006; pp. 1–5. [CrossRef]

39. Martin, A.D.; Cano, J.; Silva, J.F.A.; Vazquez, J.R. Backstepping control of smart grid-connected distributed photovoltaic power supplies for telecom equipment. *IEEE Trans. Energy Convers.* **2015**, *30*, 1496–1504. [CrossRef]
40. Pozo, B.; Garate, J.I.; Araujo, J.Á.; Ferreiro, S. Photovoltaic energy harvesting system adapted for different environmental operation conditions: Analysis, modeling, simulation and selection of devices. *Sensors* **2019**, *19*, 1578. [CrossRef] [PubMed]
41. Roumila, Z.; Rekioua, D.; Rekioua, T. Energy management based fuzzy logic controller of hybrid system wind/photovoltaic/diesel with storage battery. *Int. J. Hydrog. Energy* **2017**, *42*, 19525–19535. [CrossRef]
42. The World's Smallest Wind Turbine. Available online: http://www.solar-i.com/S&Y/wssen.htm (accessed on 19 May 2023).
43. Chiang, S.; Shieh, H.J.; Chen, M.C. Modeling and control of PV charger system with SEPIC converter. *IEEE Trans. Ind. Electron.* **2008**, *56*, 4344–4353. [CrossRef]
44. Tuna, G.; Gungor, V. Energy harvesting and battery technologies for powering wireless sensor networks. In *Industrial Wireless Sensor Networks*; Elsevier: Amsterdam, The Netherlands, 2016; pp. 25–38. [CrossRef]
45. Rabah, S.; Zaier, A.; Dahman, H. On Evaluating Energy Efficient Algorithms for Internet of Things Networks. In Proceedings of the 2019 IEEE 19th Mediterranean Microwave Symposium (MMS), Hammamet, Tunisia, 31 October–2 November 2019; pp. 1–4. [CrossRef]
46. Xu, X.; Lin, Z.; Zhou, P. Research on Vehicle Routing Problem of Multiple Oil Depot Passive Distribution under Multi Oil Supply Constraints. *Chin. J. Manag. Sci.* **2021**, *29*, 157–165. [CrossRef]
47. Hu, N.; Tian, Z.; Du, X.; Guizani, N.; Zhu, Z. Deep-Green: A Dispersed Energy-Efficiency Computing Paradigm for Green Industrial IoT. *IEEE Trans. Green Commun. Netw.* **2021**, *5*, 750–764. [CrossRef]
48. Donyaii, A.; Sarraf, A. Optimization of reservoir operation using a bioinspired metaheuristic based on the COVID-19 propagation model. *Numer. Methods Civ. Eng.* **2020**, *5*, 15–28. [CrossRef]
49. Gali, V.; Babu, B.C.; Mutluri, R.B.; Gupta, M.; Gupta, S.K. Experimental investigation of Harris Hawk optimization-based maximum power point tracking algorithm for photovoltaic system under partial shading conditions. *Optim. Control Appl. Methods* **2023**, *44*, 577–600. [CrossRef]
50. Mashayekhi, M.; Mosayyebi, S. A new hybrid Harris hawks optimization (HHO) and particle swarm optimization (PSO) algorithm for the design of castellated beams. *Asian J. Civ. Eng.* **2023**. [CrossRef]
51. Hijazi, N.; Aloqaily, M.; Ouni, B.; Karray, F.; Debbah, M. Harris Hawks Feature Selection in Distributed Machine Learning for Secure IoT Environments. *arXiv* **2023**, arXiv:2302.12205. [CrossRef]
52. Yaqoob, S.; Hussain, A.; Subhan, F.; Pappalardo, G.; Awais, M. Deep Learning Based Anomaly Detection for Fog-Assisted IoVs Network. *IEEE Access* **2023**, *11*, 19024–19038. [CrossRef]
53. Saraereh, O.A.; Alsaraira, A.; Khan, I.; Choi, B.J. A hybrid energy harvesting design for on-body Internet-of-Things (IoT) networks. *Sensors* **2020**, *20*, 407. [CrossRef] [PubMed]
54. Tran, H.T.; Nguyen, M.T.; Nguyen, C.V.; Ala, G.; Viola, F.; Colak, I. Hybrid solar-RF energy harvesting mechanisms for remote sensing devices. *Int. J. Renew. Energy Res.* **2022**, *12*, 294–304.
55. Xiao, H.; Qi, N.; Yin, Y.; Yu, S.; Sun, X.; Xuan, G.; Liu, J.; Xiao, S.; Li, Y.; Li, Y. Investigation of Self-Powered IoT Sensor Nodes for Harvesting Hybrid Indoor Ambient Light and Heat Energy. *Sensors* **2023**, *23*, 3796. [CrossRef]